UCRL-10778

University of California

Ernest O. Lawrence Radiation Laboratory

TWO-WEEK LOAN COPY

This is a Library Circulating Copy which may be borrowed for two weeks. For a personal retention copy, call Tech. Info. Division, Ext. 5545

THE SUBSTRUCTURE OF PLASTICALLY DEFORMED NICKEL

Berkeley, California

DISCLAIMER

This document was prepared as an account of work sponsored by the United States Government. While this document is believed to contain correct information, neither the United States Government nor any agency thereof, nor the Regents of the University of California, nor any of their employees, makes any warranty, express or implied, or assumes any legal responsibility for the accuracy, completeness, or usefulness of any information, apparatus, product, or process disclosed, or represents that its use would not infringe privately owned rights. Reference herein to any specific commercial product, process, or service by its trade name, trademark, manufacturer, or otherwise, does not necessarily constitute or imply its endorsement, recommendation, or favoring by the United States Government or any agency thereof, or the Regents of the University of California. The views and opinions of authors expressed herein do not necessarily state or reflect those of the United States Government or any agency thereof or the Regents of the University of California.

UCRL-10778
UC-28 Metals, Ceramics
and Materials

UNIVERSITY OF CALIFORNIA

Lawrence Radiation Laboratory
Berkeley, California

Contract W-7405-eng-48

THE SUBSTRUCTURE OF PLASTICALLY DEFORMED NICKEL

Richard L. Nolder

(Ph. D. Thesis)

April 1963

Reproduced by the Technical Information Division
directly from author's copy.

Printed in USA. Price $1.50. Available from the
Office of Technical Services
U. S. Department of Commerce
Washington 25, D.C.

THE SUBSTRUCTURE OF PLASTICALLY DEFORMED NICKEL

Richard L. Nolder

Abstract

Transmission electron microscopy techniques were used to study the substructure of pure nickel deformed under static and shock loading conditions. The shock loading was carried out under originally ambient temperature conditions. Loads ranged from 70 to 700 kilobars. Static loading involved compressive loading at the ambient temperature and tensile loading at temperatures ranging from 4°K to the ambient temperature.

A dislocation cell structure was found in all statically loaded specimens, as had been observed previously, and in specimens shock loaded up to 250 kilobars. Microtwinning was observed for the first time in nickel shock loaded at 350 kilobars and higher.

It was found that under initially ambient temperature conditions the energy input per unit volume was inversely proportional to the square of the cell diameter. A possible explanation for this was proposed, making use of Kuhlmann-Wilsdorf's theory for work hardening in which the energy required to bow out dislocation segments was equated to the inverse square of an average dislocation segment's length. A similar analysis was used to explain twinning. By making use of both analyses a quantitative relation between the average cell diameter and the average segment length was predicted which seemed consistent with observations. A prediction of the ratio between the rigidity modulus and the work hardening coefficient in Stage II of work hardening was consistent with actual measurement obtained from published data. It is proposed that this type of analysis should be applied to other metal systems.

INTRODUCTION

The many methods of stress application may be divided into two broad categories. In one case, a load is applied in such a gradual manner that the stresses within a body are considered to be instantaneously distributed to all points. This is referred to as static loading. If, on the other hand, a stress is applied abruptly or is changing abruptly, the propagation of stress waves through the material must be considered. Such a stress application is referred to as shock loading.

Static loading of materials has been the subject of by far the majority of books and papers concerning mechanical properties. On the other hand, even though during the nineteenth century a theory was developed for the propagation of elastic shock waves in solids, very little investigation of shock loading was carried out until World War II. This was primarily because of experimental difficulties and a lack of interest. Within the last twenty years, with the development of new materials and experimental techniques as well as an increasing number of problems concerning high rates of loading, there has been a revival of effort in the theoretical and phenomenological study of shock waves and shock loading. This included the development of theories for plastic wave propagation pioneered by Taylor,[1] von Karman and Duwez,[2] and Rakhmatulin,[3] with later improvements by Malvern.[4] The primary interest in dynamic loading concerns the application of pressures which are far higher than the yield strength of materials under static loading conditions. Such shock waves are usually produced by an explosive charge, other methods being the use of high velocity projectiles, discharge of high energy capacitor banks, and short pulse magnetic induction.

The primary difficulty with the existing theories of plastic wave propagation concerns the fact that it is necessary to make assumptions

concerning the plastic behavior of materials. When dealing with crystalline materials, it is necessary to consider the crystalline imperfections such as dislocations, grain boundaries, point defects, etc., and their effect on deformation mechanisms. Therefore, any assumptions are limited by the knowledge of these effects. At present, some information is known concerning dislocation mechanisms and a recent paper by Dorn and Hauser[5] points out the relevance of these mechanisms to the plastic wave theories. Of course, there is a great deal of effort being made to further understand these mechanisms and much further progress is anticipated.

It has generally been recognized by metallurgists that there is a need to understand the physical condition of metals in the shock wave. Since a shock wave is of short duration, small thickness, and has an extremely high rate of propagation, only indirect evidence has been available concerning its nature. Usually such information is obtained by correlating the load conditions (pressure, application time, etc.) with the final structure of a shock loaded material. Since it is advantageous to work with the conditions of planar wave propagation where only time and a linear coordinate system describes the propagation, most scientific work makes use of plane wave generators or very similar techniques in the shock loading of materials. A description of such a generator will be presented later.

If proper precautions are taken to avoid spalling, a metal loaded by means of a planar wave has the general properties that there has been very little change in the dimensions of the sample and no detectable change in grain size or shape. In contrast, the hardness of the sample has been raised considerably (as much as two or three times on the DPH scale). The microstructure of a sample contains slip lines, twin structures and, in the case of iron, a structure very similar to martensite. In other words,

the results of diffusionless shear type reactions are observed as might be expected from such high valued, short duration stress load. In the case of face-centered cubic metals of high stacking fault energy, such as aluminum and nickel, no twins had been observed in the microstructure even at high shock pressures prior to the work presented here. It seemed, therefore, that the structure of such metals might be ideal for studying the effect of dislocation structure caused by shock loading without the complications of the other microstructures mentioned. A primary method for studying the substructure of metals is the use of transmission electron microscopy techniques.(8) This involves obtaining a metal thin enough to allow transmission of a beam of electrons. By using this technique, much valuable information can be obtained regarding the substructure of metals, e.g., dislocations, ordering, twinning, etc., both from studies of image contrast effects and selected area diffraction patterns.

The majority of the studies of shock loaded metal structures has been carried out by means of light microscopy techniques. At least one investigator(6) has made use of electron microscopy using replica techniques. It is understood by the author that there are a number of investigators at present using transmission electron microscopy techniques to study the submicroscopic structure of shocked metals, but at present there is only one group of investigators, Leslie, Hornbogen and Dieter,(7) who have reported their work in the literature. Since their investigation concerned the structure of shock-hardened iron, their primary concern was with the martensite-like structure found in this material. Only at relatively low pressures were they able to study dislocation arrangements without the complication of other structure effects. In the work presented here, transmission electron microscopy was used to study the substructure of shock loaded pure

nickel, which, as already stated, was not expected to have the above complications. A comparison was also made between this structure and that found in statically loaded nickel. It will be shown in this report that, as expected, many different types of structure are produced in this material than were found by Leslie et al. in iron.[7] The primary dislocations structures found in statically loaded metals may be divided into two main groups which depend on the stacking fault energy of the metal involved. In low stacking fault energy materials ($\gamma < 20$ ergs/cm^2, e.g., α brass) we find stacking faults bounded by partial dislocations and dislocations are arranged in pile-ups. In metals having intermediate or high stacking fault energy ($\gamma > 20$ ergs/cm^2, e.g., Cu $\sim$ 40, Ni $\sim$ 80) pile-ups are not observed. In the latter case, dislocations are relatively free to change glide planes and, instead of forming pile-ups, dislocations tangle and form walls of dislocations. By means of transmission electron microscopy these walls are observed to enclose cells which are regions relatively dislocation-free. It is this type of structure which has been observed and studied in this work. In addition, some very unexpected results were found which involves a microtwinning structure.

MATERIALS AND PROCEDURES

Observations were made of specimens deformed by means of shock loading and compression at the ambient temperature, and tensile deformation at temperatures ranging from 4°K to the ambient temperature.

Materials

Two forms of high purity nickel were used. A two-inch diameter round bar was used for all investigations involving shock or compressive loading. All tensile deformation was performed with samples prepared from 2-inch wide, 0.1-inch thick rolled sheet. The chemical analysis for the bar stock was

.003% C, .001% Mn, .0004% Fe, 001% S, 0006% Si, .001% Cu, 0001% Cr, and .0004% Co by weight. For the rolled sheet it was .020% C, .001% S by weight with traces of Co and other impurities.

Deformation Specimen Preparation

Samples prepared from the bar were obtained by slicing perpendicular to the axis of the bar and lightly machining the cut faces until they were parallel. All shock loaded specimens were $\frac{1}{4}$ inch thick. Their complete preparation to the shock loaded state was carried out by Arthur D. Little, Inc. Compression specimens were $\frac{1}{4}$ to $\frac{1}{2}$ inch thick prior to mechanical deformation. Tensile specimens were prepared by rolling the original sheet to a .011-inch thickness and cutting out one-inch wide specimens (the length being parallel to the rolling direction) from the center portion of the sheet.

All specimens were annealed at 925°C for 3 hours and furnace cooled in vacuum prior to being mechanically deformed. One of the bar specimens was retained in the annealed state for later comparisons with deformed specimens.

Grain Size

Sections parallel to the axis of the annealed bar stock when etched for grain size revealed that the outer portions contained coarse grains. The coarse grain structure was about $\frac{1}{2}$ inch thick with the grain size gradually increasing toward the center of the bar. Further toward the center the grain size abruptly became extremely fine and uniform. This structure was attributed to the greater work hardening received at the surface during forming, which gradually decreased toward the center of the bar, with its ultimate effect on the recrystallization. Impurities may also be responsible for this structure, e.g., as a result of segregation.

Care was taken to make the observations described here in the fine grain portion of all specimens. The fine grain area had an average grain diameter of 60μ. The grain diameter of the tensile specimens was uniform, having an average of 31μ.

Etching was done electrolytically by first electropolishing for 2 minutes at room temperature and 4.5 volts in a 60% sulfuric acid solution containing 5 grams per liter P-toluenesulfonic acid followed by a reduction of the voltage to 1.5 volts for 30-60 seconds.

Loading Techniques

Shock loaded specimens were impacted at pressures of 70, 130, 250, 350, and 700 kilobars along the axis of the bar. The degree of error in these pressures were approximately ± 20 kilobars. Since the author never participated in the loading of these specimens, only a second-hand account of the preparation of these specimens can be given. The majority of the details are presented as a quotation from a personal communication from Arthur D. Little, Inc.

> "The required plane shock waves were produced by means of chemical sheet explosives supplied by E. I. du Pont de Nemours & Co. The generator makes use of their line wave initiator which is a triangular sheet of explosive with a series of accurately spaced holes. A detonation wave initiated at the apex of the triangle requires the same time to reach the opposite side along any possible path. The detonation front, therefore, reaches all points of the base of the triangle simultaneously. The line wave initiator detonates one edge of a square sheet of PETN explosive, supported by a glass plate and separated from the main explosive charge by wooden angles. The detonation front propagates as a line down this top sheet, projecting glass fragments downward onto a second sheet of explosive supported by a glass plate. Sheets of explosive below this second glass plate form the main explosive charge. The angle of the top explosive sheet is adjusted so that the glass fragments arrive at and detonate the 5-inch square top surface of the main explosive charge simultaneously. The main explosive charge generates a plane shock wave in a copper driver plate."

The copper driver plate then collides with the specimen assembly transmitting a shock wave. A sketch of the relationship of the driver plate and the specimen assembly is shown in Figure 1.

"The assembly is designed to load the specimens with a planar shock pulse of desired magnitude in such a way that it can be recovered essentially undamaged. Provision must be made to remove the highest pressure portion of the shock wave before it can propagate intense tensile waves, and for this purpose, the spall plate (nickel) is placed as shown. It is fragmented quite completely and the rarefacations (also tensile) developing at lateral extremities are avoided by the use of inserted pellets. Such interfaces are essentially opaque to tensile waves, but transparent in compression so they tend to act as one-way valves. The entire specimen assembly is made of nickel to avoid reflections due to acoustic mismatch. The shock wave pressures generated by this system were varied by altering the thickness of the main explosive charge, the thickness of the driver plate, and the stand-off distance."

Static compression loading was carried out parallel to the bar axis with a Baldwin-Tate-Emery universal testing machine using a loading rate of 20,000 pounds per minute. Two compression specimens were prepared. One specimen was deformed to a load of 150,000 pounds or 44,000 psi and a true strain of 10%. The other received a load of 550,000 pounds or 102,000 psi. This produced a true strain of 60%.

Tensile specimens were deformed on the Instron Universal testing machine. A one-inch gauge section was used with a relative head movement rate of 2×10^{-2} inches/min. Five specimens were prepared for observations. Four specimens were deformed to 20% strain, one each at the temperatures 4°, 78°, 195° and 295°K. One specimen was deformed 32% at 78°K. The sub-ambient temperatures were obtained by the use of liquid baths, 4°K by means of liquid helium, 78°K by means of liquid nitrogen, 195°K by means of solid carbon dioxide in ethyl alcohol. 295°K was an ambient temperature.

Spark Erosion Cutting Technique

In order to prepare foils suitable for transmission electron microscopy from the annealed, shock-loaded, and statically compressed round bar specimens, thin sections were cut parallel to the bar axis which was also the compression direction. In order to obtain strain-free samples, cutting was carried out by means of spark-erosion using the Servomet Spark Machine.* In this spark erosion system a tool and the work are submerged in a dielectric, kerosene, and maintained as electrodes of opposite sign. Erosion of both pieces occurs by means of spark discharges. The movement of the tool relative to the work is controlled by a servo system which maintains the work gap at an optimum value by sensing the dielectric breakdown voltage across the work gap. The cutting rate of the process, for a given work surface, is largely a function of the intensity and frequency of the spark discharge, which in turn are dependent upon the storage capacity and time constant of the selectable resistance-capacitance elements in the power supply.

Usually a blade type tool is used for cutting a specimen. However, as tool depth into the sample increases, energy dissipation occurs not only at the cutting edge but also along the sides of the tool which have become in close proximity to the cut faces. Besides the fact that a great deal of cutting power is lost by such extra energy dissipation, it is difficult to cut a uniform slice, since upper portions of a slice become eroded to a greater extent than lower portions.

In order to avoid these difficulties a tool was used which was a tensioned wire transported across the specimen at a steady rate in order to avoid loss of dimensions due to erosion. This tool is illustrated in Figure 2. It is seen that the cutting wire (A) is supplied from a spool (B)

* Manufactured by Metals Research Ltd., Cambridge, England.

transported over glide pulleys (C) by a motor driven transport mechanism (D). A tensioning device (E) permits optimum wire tension adjustment. The entire assembly is carried by the servo-controlled tool mount (F).

Parallel cuts were made by first making one cut, then moving the specimen mount perpendicular to the cutting direction by means of a screw drive. The distance moved was equal to the desired thickness of the slice plus the diameter of the wire and twice the spacing between the wire and the specimen during cutting. Another cut was then made which was parallel to the first. By this method parallel slices approximately .010" thick were obtained.

The smallest cutting rate available on the Servomet Spark Machine was employed during the parallel cutting in order to minimize any possible mechanical damage to the specimens. As will be indicated shortly, no significant contribution was made to specimen substructure by this cutting operation.

Thin Foil Preparation

In order to obtain thin foils suitable for transmission electron microscopy, the slices as well as the tensile specimens were electropolished using the solution described previously for grain boundary determination. A solution temperature of 5-10°C and 4.5 volts with a stainless steel cathode were the polishing conditions used.

The window method[8] was employed. The specimens were initially lacquered around all the edges with Lacomit,* leaving a portion of the foil bare, which was the exterior anode contact. The specimens were then electropolished until perforation occurred. Specimens which were considered thin enough for electron transmission (1000-4000 Å) were carefully cut off by means of a scapel. If further polishing was to be carried out, the

* Manufactured by W. Canning and Co., Ltd., Birmingham, England.

perforated edges were covered with lacquer. In this manner the current distribution on the foil was kept as uniform as possible.

Specimen Examination

The foils were examined in a Siemens Elmiskop I b electron microscope. An electron accelerating voltage of 100 kV and a projector pole piece of 0.77 mm diameter were employed. Foil orientations were determined by the selected area diffraction technique.

Hardness Tests

Micro-hardness tests were performed on the annealed, shock loaded and compressively loaded specimen sections remaining after thin slices were obtained. These sections were electropolished for two minutes using the same solution conditions described for the thin foil preparation. Diamond Pyramid Hardness Numbers were obtained using the Kentron Micro Hardness Tester with a 136° diamond pyramid indenter and a 500 gram load. Hardnesses were obtained approximately every .015 inches along the original axis of the bar material.

OBSERVATIONS AND RESULTS

Specimen Hardness

The summary of the hardness measurements is shown in Figure 3. The Vickers Hardness is plotted versus the applied load. The mean of the hardness values as well as the 95% confidence limits are given for each specimen. There was no significant variation in the hardness values along the thickness of any specimen. It is seen that for the same loading pressure, static loading produces a much greater hardness than shock loading. In contrast, it will be shown later that for the same amount of strain, a shock loaded specimen is much harder than a static loaded specimen. These are typical

observations of the relations between the hardnesses of static and shock loaded specimens as illustrated by Dieter's work[6] on nickel.

It is shown that a smooth curve may be drawn through the mean hardness points of the shock loaded specimens up to 250 kilobars. There then appears to be a sharp break in the hardness trend between 250 and 350 kilobars. This is typical of an abrupt change in structure character or mode of deformation. It is interesting that a similar break may be interpreted from the hardness data presented by Dieter[6] in his work on nickel. This is shown in Figure 4. It will be shown later that there is indeed a significant difference between the structures of the specimens loaded to 250 kilobars or below, and that of the 350 and 700 kilobar specimens. It is seen that the hardness of the 350 and 700 kilobar specimens are approximately the same with 700 kilobar specimen having the lower hardness.

Transmission Electron Microscopy Observations

All substructures observed in the deformed specimens were much more complicated than the dislocation-free structure observed in the annealed specimen typified in Figure 5. Since this annealed sample was taken from the annealed bar specimen by means of the spark erosion technique described, it received all treatments employed in foil preparation. This indicates that no appreciable mechanical damage was administered to the specimens in their preparation for observation.

Transmission electron microscopy of all deformed specimens excluding the 350 and 700 kilobar shock loaded specimens revealed a structure of densely tangled dislocations primarily arranged in cell walls enclosing areas relatively free from dislocations. This is similar to the structure commonly observed in statically deformed nickel as well as in many pure metals, both FCC and BCC,[9] particularly when they are deformed at ambient temperatures.

It should be pointed out that such a cell structure differs from the model for compressive shock proposed by C. S. Smith[10] in which the moving interface between the undisturbed and compressed materials is considered to be composed of two sets of inclined edge dislocations. This model assumes that a high density of these dislocations exists within the shock front with none remaining after the passage of the shock wave.

The cell structure is also different than the dislocations structure observed by Leslie, Hornbogen and Dieter[7] in iron at low shock pressures. They found that long dislocations were present in their micrographs. Hornbogen[11] found that these dislocations were mostly of a screw type. He proposed that such a substructure may be due to the movement of edge components of dislocation loops formed as a result of the compression wave. He assumed that these edge components moved with the velocity of the shock front leaving behind screw components.

a) Shock Loaded Specimens. Typical micrographs of the 70-250 kilobar specimens are shown in Figures 6a-c. It is seen that the cell diameter decreases with increasing pressure. In fact, in the 250 kilobar micrograph it appears that any form of cell structure is completely absent. However, at the higher magnification of the same area shown in Figure 7, there appears to be a general form of a cell structure existing in this specimen. A number of dislocations within the cell walls of these specimens, as well as those in the low temperature tensile specimens, appear to have a uniform directionality. However, attempts to relate crystallographic directions with these directions, which might show the dislocations to have primarily edge or screw character, have been unsuccessful.

The 350 and 700 kilobar specimens had structures which were more complicated than those of the other specimens. These structures can be divided into three groups, twinning, thin distorted regions (elongated subgrains)

and a dense dislocation structure in the background. The twinning, which lies along {111} planes, is of particular interest since Dieter[6] was unable to observe twinning in his experiments using both light microscopy and electron microscopy of replicas. As shown in Figure 8, a micrograph of a (110) orientation, the twins are extremely fine (0.05μ thick) and thus would not be resolvable by light metallography. In Figure 9b there appears to be a high density of dislocations at the twin-matrix interface suggesting that the twins may be incoherent. Figure 9a shows the electron diffraction pattern of Figure 9b. The foil is in the $(5\bar{1}0)$ orientation, and the spots marked T_1 and T_2 are the reflections corresponding to the two sets of twins in Figure 9b. T_1 has the orientation $(13\bar{4})$ and T_2 (134). The contrast can be reversed for either set by means of dark field illumination using the diffraction spots corresponding to that set. The spots not corresponding to any of the three lattices are attributed to double diffraction.

Figure 10 is an example of another area of the same specimen from which Figure 9 was obtained in which twinning is not present. The structure here consists of elongated subgrains and a dense background of tangled dislocations.

Another typically distorted region is shown in Figure 11a. The elongated subgrain is parallel to the trace of a (111) plane. It can be shown that this area is a highly distorted single crystal by means of its selected area diffraction pattern and dark field examination. The diffraction pattern is shown in Figure 11b. It is seen that some matrix reflections are split into many spots indicating misorientation from subgrain to subgrain. Dark field observations enable one to associate each of these spots with a subgrain in the long thin distorted region, while dark field observations using single well-defined spots reveal a dark area in this region. This is typical of heavily worked metals.[12,13]

b) Statically Compressed Specimens. A typical cell structure of the specimen strained 10% compressively is shown in Figure 12. The cell diameter was in general much larger and well-defined than the shock loaded specimen. The cell walls appeared to form along well-defined directions. Warrington in this work[14] found that the cell walls in copper tended to lie along {100}, {110} and {111} planes, particularly at elevated temperatures. In this work, definite crystallographic directions could not be satisfactorily associated with the axes of cells in the compressed specimens. However, in the tensile specimen a very definite crystallographic relation was found which will be shown shortly.

Figure 13 is a micrograph of an area from the 60% compressively strained specimen. Two adjoining grains are shown. The direction of compression is indicated. It is seen that the cell structure is elongated perpendicular to the compressive direction. This elongation is very similar to the dimensional elongation of the grains observed in the same specimen. Within each grain there is a great deal of distortion as indicated by the changes in contrast within and between cells. In very few cases was it possible to obtain a well-defined selected area diffraction pattern due to this distortion. The cells were smaller than those found in the 10% specimen.

c) Tensile Specimens. A typical micrograph of the ambient temperature specimen is shown in Figure 14. The plane of this area is (001) with the two <100> directions indicated. The structure is similar to that of the 10% compression specimen both in the size of the cell and the cell wall texture. It is seen that a large number of cell walls are aligned along {100} planes. A great number of areas of (001) orientations were observed. This should be expected since "cube texture" is quite prevalent in many cold rolled

and annealed face-centered cubic metals, including nickel.[15] This texture involves preferred orientation in which the rolling plane contains primarily {100} orientations and the rolling direction has primarily <001> directions along it. The reason for the alignment of cell walls only along {001} planes, excluding the {110} and {111} planes observed by Warrington in copper,[14] is not understood at this time.

In micrographs of specimens deformed at lower temperatures the cells were decidedly smaller and the cell walls were less defined than those statically deformed at room temperatures. There is also a tendency for the cell walls to be aligned with the <100> directions but to a lesser extent than at room temperature. This is again consistent with the observations made for copper by Warrington.[14] The structures of the low temperature specimens were similar in many ways to that of the shock loaded specimens. Besides having a cell size similar to the 70 kilobar specimen, the cell walls also contained a large number of dislocation in parallel directions. A typical micrograph for the specimen deformed 20% at 78°K is shown in Figure 15. This is very similar to the samples deformed 20% at 4°K and 195°K. When foils of the specimen deformed 32% at 78°K were observed, it was found that the contrast was always dark irrespective of orientation. This means that electrons were scattered in all directions by the sample because of the misorientations caused by a large dislocation density. Such micrographs were difficult to interpret. However, information could be obtained concerning the cell size. The cell size in this specimen was smaller than in the specimen deformed 20%.

Quantitative Analysis of Cell Size

Included in the description of various cell structures have been statements concerning the relative sizes of cells produced by different treatments. These conclusions can be made in a qualitative manner by just

comparing many micrographs of each specimen. However, when individual cells were actually measured a broad range of diameters was found within each specimen. This is indicated by the values found in the far right columns of Table I which is a compilation of the statistical data obtained from many micrographs. Although the general trends which were previously cited are also present in this list of ranges, more definitive values were obtained when the average cell diameters from each micrograph were treated statistically. Therefore, both the means of these averages and their 95% confidence limits are also listed in Table I. An analysis of these means will be presented in the discussion to follow.

DISCUSSION

Previous workers[14, 16] have shown that the diameters of cells found in both FCC and BCC metals can be related to the amount of strain a material receives, the stress level to which it is raised, and the deformation temperature. Qualitatively their findings correlate with the data presented in this work. Warrington[14] found that in copper a linear relation exists between the inverse square root of the cell diameter and the flow stress. He pointed out that this is similar to the well-known relation between grain size and flow stress. Such a relationship was not found to be the case in shock loaded nickel. It was also found that the inverse of the cell diameter increased much more rapidly with applied stress for the statically loaded nickel in a manner similar to the variation with Vickers hardness. (Figure 3)

Relationships of much greater interest and heretofore not known were found when the inverse square of the cell diameters was plotted against the work per unit volume applied to the specimens. Such a plot is shown in Figure 16. For the statically loaded specimens this amount of work was obtained by integrating stress-strain curves obtained during deformation. The method used for the shock loaded specimens is described in Appendix A.

TABLE I

Cell Diameter Statistics

Specimen	Mean Diameter(μ)	95% Confidence Limits of the Average Cell Diameter High(μ)	Low(μ)	Range of Cell Diameters High(μ)	Low(μ)
Shock Loaded					
70 K Bar	.530	.690	.365	1.60	.135
130 K Bar	.315	.332	.297	.450	.175
250 K Bar	.167	.170	.163	.250	.07
Compressed					
10% Strain	.890	1.070	.710	3.00	.30
60% Strain	.545	.643	.406	2.69	.125
Tensile					
20% Strain					
295°K	.825	1.00	.645	2.50	.20
195°K	.530	.625	.430	2.00	.10
78°K	.490	.625	.350	1.67	.12
4°K	.495	.620	.370	1.25	.125
32% Strain					
78°K	.330	.376	.282	1.10	0.10

We can see that at the ambient temperature, irrespective of the method of deformation, the relationship between the inverse square of the cell diameters and the applied work is linear and passes through the origin. With the small amount of low temperature data available, it appears that the slope of this line increases with decreasing temperature. This temperature effect is very small below 195°K. Below 78°K it is negligible. This is illustrated in Figure 17, where cell size is plotted versus temperature for specimens deformed 20%.

One explanation for these relationships can be derived from a recent theory on work hardening presented by Kuhlmann-Wilsdorf.[17] The portion of this theory pertinent to this explanation is outlined in Appendix B. Using the terms described in Appendix B, we see that the strain increment due to the bowing out of dislocation segments can be expressed as $d\gamma = \frac{K}{G} d\tau_{\bar{\ell}}$ and, therefore, the integral $\int \tau_{\bar{\ell}} \, d\gamma$ may be written $\frac{K}{G} \int \tau_{\bar{\ell}} \, d\tau_{\bar{\ell}}$. Since $\tau_{\bar{\ell}} \doteq \frac{Gb}{h\bar{\ell}}$, the integral can be written $\frac{KGb^2}{h^2} \int -\frac{d\bar{\ell}}{\bar{\ell}^3}$ Since the flow stress is proportional to $\frac{1}{\bar{\ell}}$, deformation in an annealed specimen occurs by bowing of the longest free segments. The energy input required to obtain a state where the average segment length is $\bar{\ell}$ is given by

$$E = \frac{K\,Gb^2}{h^2} \int_{\infty}^{\bar{\ell}} -\frac{d\,\bar{\ell}}{\bar{\ell}^3} = \frac{K\,Gb^2}{2h^2\,\bar{\ell}^2} \qquad (1)$$

We see that the theory predicts a linear relationship between the energy input and the inverse square of the average segment length. This relationship is in fact observed experimentally since tangles in cell walls appear to act as sources. Such a possible source is illustrated in Figure 18. We need only add the assumption that the average cell diameter is directly proportional to the average active dislocation segment length. The temperature effect observed in the cell size energy relations appears to be

mainly accounted for by the temperature dependence of the terms contained in K, particularly the $\frac{\alpha}{\beta}$ terms explained in Appendix B.

Although we have made what appears to be a very good correlation between our observations and Kuhlmann-Wilsdorf's theory, (some of which are surprisingly quantitative as will be shown shortly) it should be emphasized that many assumptions have been made. In particular, the calculation of the energy input for the shock loaded specimens is considered to be, at best, an estimate and is not accepted by all workers. However, it is the only approximation possible at the present time. The assumption that the shock loaded specimens were plastically deformed at nearly room temperature is not confirmed by thermodynamics. Calculations show that the theoretical temperatures[18] rise as high as 100°C in a 250 kilobar specimen with a final temperature of 45°C after the adiabatic expansion. It is also understood by the author that unpublished data indicate that specimen temperatures may even go higher than the thermodynamic calculations. Since at present the mode of deformation and the temperature effects involved are still speculative, it is felt that our assumptions may be used, particularly in the strength of the resulting correlation with experiment and theory.

It is well known that twinning occurs at low temperatures in FCC metals[19] as well as at shock loading pressures.[20] It has been usually assumed that twinning is an athermal effect which occurs at a critical stress. From the information we have shown here concerning the relationships of energy and cell size, it is of interest to see if a similar relationship can be found concerning twinning. Several mechanisms have been proposed[21,22,23] for the formation of twins. In all cases, it has been assumed that the nucleation of twins occurs by the formation of stacking faults. The essential difference between the mechanisms of Venables[21] and Suzuki[22] is that while the latter

involves a pair of twinning dislocations moving away from a Cottrell-Lomer barrier and the twinning energy is the important term, in the former, extended jogs in glissile dislocations are presumed to be the source of twin nuclei and the stacking fault energy is the important term. A very recent model[23] is based on the simultaneous splitting of a large number of dislocations in a pile-up. Our results show that twinning occurs when dislocations become extremely closely spaced and that many of the twins are incoherent as expected from the Cohen-Weertman model.[23] Until now, it has not been possible to decide which mechanism (or all of them) is the most important. According to Venables, the stress required to activate a twinning dislocation of length ℓ is

$$\tau_T = \frac{S}{b_1} + \frac{p\ G\ b_1}{\ell} \tag{2a}$$

where b_1 = the Burgers vector of the Shockley partial

S = the stacking fault energy of the metal

p = a constant of the order of unity.

In Suzuki's theory,

$$\tau_T = \frac{S}{2b_1} + \frac{Gb_1}{\ell} \tag{2b}$$

We see that these expressions resemble that for the stress required to activate dislocation loops as presented in Appendix A. If we perform a similar analysis, we find that the energy required to activate an average dislocation length of $\bar{\ell}$ for both cases (2a) and (2b) would be

$$E_T = K\left(\frac{S}{h\bar{\ell}} + \frac{Gb_1^2}{2h^2\bar{\ell}^2}\right) \tag{3a}$$

and

$$E_T = K\left(\frac{S}{2h\bar{\ell}} + \frac{Gb_1{}^2}{2h^2\bar{\ell}^2}\right) \tag{3b}$$

We would expect twinning to occur when the average dislocation length was such that $E_T \leq E$, i.e., when

$$S \leq \frac{G}{2h\,\bar{\ell}}\,(b^2 - b_1{}^2) \quad \text{in Venables' model} \qquad (4a)$$

or

$$S \leq \frac{G}{h\,\bar{\ell}}\,(b^2 - b_1{}^2) \quad \text{in Suzuki's model} \qquad (4b)$$

On this basis, a metal would twin when $\bar{\ell}$ was reduced to a value satisfied by the above equations. Before this value was reached a dense dislocation structure (a cell structure in many cases) would be produced.

In the case of pure nickel, if one takes the following values for the parameters given:

$$S = 80 \text{ ergs/cm}^2$$

$$G = 7 \times 10^{11} \text{ dynes/cm}^2$$

$$b^2 = \frac{a^2}{2} \text{ where a is the lattice parameter}$$

$$b_1{}^2 = \frac{a^2}{6}$$

$$a = 3.5 \times 10^{-8} \text{ cm}$$

we obtain a value for $h\,\bar{\ell}$ equal to 0.018 μ from (4a) and 0.036 μ from (4b). If we assume that h = 1 and that $f\bar{d} = \bar{\ell}$, where f is a proportionality constant and $\bar{d}$ is the average cell diameter, we see that $f\bar{d}$ is either 0.018 μ or 0.036 μ. Experimentally, we see that at the ambient temperature a twin structure is not produced until a specimen is shock loaded to a pressure somewhere between 250 and 350 kilobars. Extrapolating the ambient temperature line shown in Figure 16 above the 250 kilobar point, we can estimate that the cell diameter where twinning would first take place is somewhere between .130 and .170 μ. Assuming a cell diameter of .150 μ, we see that the term f would have a value of approximately $\frac{1}{4}$ or $\frac{1}{8}$. Following the logic of our derivations, $\bar{\ell}$ is $\frac{1}{4}$-$\frac{1}{8}$ the size of $\bar{d}$. This is certainly a reasonable value. In fact, we see many cases such as illustrated in Figure 18 where loops of this order of size do bow out from the cell wall toward the center of a cell.

One can easily imagine that such loops could interact with other loops to reduce the size of a cell as deformation proceeds. At higher temperatures more of these loops would be annihilated and therefore would not contribute to the reduction in cell size.

Since Kuhlmann-Wilsdorf[17] predicts that the constant K should be approximately 300, it is of interest to make a calculation of this term using our experimental interpretation of this theory. Since there is negligible temperature effect in slope of the inverse square diameter-energy line between 4° and 78°K, this appears to be a good value in estimating the value of K expected in Stage II of slip. We see that when $E = 10^5$ in-pounds/in.^{3}, $\frac{1}{\bar{d}^2} = 85\mu^{-2}$. From equation (1)

$$K = \frac{2h^2\ \bar{\ell}^2\ E}{Gb^2} \qquad (5)$$

and substituting fd^2 for $\bar{\ell}^2$ we find that K has the value of 59 on Venables' model or 238 on Suzuki's model. This latter value is in the range predicted by Kuhlmann-Wilsdorf and is therefore consistent with the assumptions made. It would appear therefore that analytically better agreement is obtained between our experimental results and the latter theory. However, it must be pointed out that the assumption that the parameter h is unity may be quite incorrect. For example, if h is 0.5, Venables' model would fit our results better than Suzuki's. One cannot, therefore, yet decide which twinning mechanism is the more important here.

A determination of the value of K can also be made from data reported by Haasen[24] on the deformation of nickel single crystals at low temperatures. His data contains the plot of 9 crystals deformed at 20° and 78°K. Calculating the values of θ_{II} from the slopes of his stress-strain curves, a value of K = 250 ± 33 is obtained. Such an extremely close experimental correlation is indeed much better than anticipated considering the approximations which have been made.

From the interpretation made here one should be able to predict in advance what average cell size should be found, or when twinning should occur under given conditions. For instance, for nickel one would expect twinning to occur at 78°K or lower temperatures with an energy between 40,000 and 70,000 in-pounds/in.^{3}, since this is the predicted energy to form an average cell diameter of between .170 and .130μ. There is only one previous instance where the mechanical twinning has been reported in nickel. Haasen[24] found that twinning occurred in the necked region of fractured single crystals at 4° and 20°K. Examining the stress-strain curves for these crystals it was found that the energy to cause fracture was about 30,000 in-pounds/in.^{3}. Since the energy would be higher in the necked portion of the crystal and one would expect the energy requirement to be lower in a single crystal specimen than in a poly-crystalline specimen, this value does not seem inconsistent with the interpretation which has been presented here.

It would be of interest to apply this interpretation to another metal, particularly one in which twinning occurs at lower energy. Copper appears to be a good possibility, since it is known to twin both under the conditions of shock loading and low temperature deformation. The possibility should be mentioned that if this interpretation is applicable to a number of metal

systems one may be able to use it as a method of measuring or estimating the stacking fault energy of metals.

Another type of investigation which should be of interest is to determine the stored energy which is created by deformation, particularly in relation to cell size and the effect of temperature of deformation. Since stored energy is regarded to be associated with the dislocations present due to deformation and Kuhlmann-Wilsdorf[17] has proposed the possibility that the ratio of stored energy to applied work may have a proportionality relation to $\frac{1}{\bar{\ell}}$, such a study could prove profitable.

Since a temperature effect has been found in the energy per unit volume-inverse square cell diameter relationship, the possibility of an associated activation energy was investigated. Using the relation

$$K(T) = \frac{2h^2 \bar{\ell}^2 E}{Gb} \qquad (6)$$

and the fact that K was found to be insensitive to temperature between 4° and 78°K we can assume that K(T) contains two terms, K'(T) and K", the latter being temperature independent. We can further assume that $\frac{1}{K'(T)}$ is the portion of dislocations not annihilated and $1 - \frac{1}{K'(T)}$ is the fraction of dislocations annihilated by temperature effects, e.g. recovery. Therefore, $1 - \frac{1}{K'(T)} = C \exp(\frac{-\Delta H}{RT})$ where ΔH is the activation energy for this annihilation and R is the gas constant. $\frac{1}{K'(T)}$ can be obtained by normalizing the $\frac{1}{\bar{d}^2}$ at each temperature for a given energy per unit volume. This can be done by using a normalizing factor which will make the $\frac{1}{\bar{d}^2}$ at 78°K equal to one. A plot of $1 - \frac{1}{K'(T)}$ versus $\frac{1}{RT}$ will then have a slope equal to $-\Delta H$. Insufficient data was available to satisfactorily carry out such an analysis in this work. Only two points could be obtained (at 195°K and 295°K) with which to determine a slope. Both points intermediate to these temperatures and above 295°K would be necessary to thoroughly investigate

any possible activation energy or combination of more than one. However, the two points indicate an activation energy of about 2000 cal/gram atom or 0.09 e.V. This is an extremely small value and cannot be associated with many mechanisms associated with dynamic recovery such as cross slip (unless stress aided). It could perhaps be associated with recovery due to the interaction of point defects and dislocations, but no definite model is proposed in this work. Perhaps, if the cell size formed at higher temperatures were studied, activation energies usually associated with dynamic recovery and recovery in general might be measured.

APPENDIX A

Shock Loading Energy Input Approximation for Plastic Deformation

It is assumed that a shock wave consists of three parts, the shock front which is the boundary between the material still in its initial state and the shock wave, the main shock wave which is under conditions similar to that of hydrostatic compression, and a rarefacation boundary between the shock wave and the material in its final state. Since in the main shock wave only hydrostatic compressive conditions are assumed, plastic deformation can take place only in the two boundaries. Arthur D. Little, Inc.[25] has made an approximation of the amount of strain involved using the arguments presented by D. S. Wood.[26]

Considering a planar shock wave, it is assumed that compression is accomplished entirely by a strain ϵ_N, whose direction is normal to the plane of the shock wave. Also,

$$\epsilon_N = \epsilon_N^{\ e} + \epsilon_N^{\ p} \qquad \text{(A-1)}$$

where $\epsilon_N^{\ e}$ is the elastic and $\epsilon_N^{\ p}$ is the plastic strain. The lateral strain, ϵ_L, is zero in all directions. Therefore,

$$\epsilon_L = \epsilon_L^{\ e} + \epsilon_L^{\ p} = 0 \qquad \text{(A-2)}$$

It is assumed that only the elastic strains produce a change in density. Therefore,

$$\epsilon_N^{\ p} + 2\epsilon_L^{\ p} = 0 \qquad \text{(A-3)}$$

Combining (A-2) and (A-3) and rearranging we see that

$$\epsilon_L^{\ e} = -\epsilon_L^{\ p} = \tfrac{1}{2}\,\epsilon_N^{\ p} \qquad \text{(A-4)}$$

In the case of triaxial compression

$$\epsilon_L^{\ e} = \tfrac{1}{3}\,\ell n\,\frac{V}{Vo} \qquad \text{(A-5)}$$

where V_o is the initial volume and V is the volume under a given compressive stress. Therefore,

$$\epsilon_N^{\,p} = \frac{2}{3}\,\ell n\,\frac{V}{V_o} \qquad \text{(A-6)}$$

The same amount of strain is assumed in the rarefacation boundary.

This is the strain commonly used for shock loading and has been derived by at least one other method.[26] The values of $\frac{V}{V_o}$ can be obtained from a Hugoniot curve for a particular metal which represents the P-V relations obtained during shock loading. The Hugoniot curve for nickel[18] is shown in Figure A-1.

In order to obtain the energy input required for plastic deformation due to shock loading, the pressure-strain curve shown in Figure A-2 is assumed. Integrating, we obtain

$$\epsilon^{p}_{shock} \approx P\,\frac{2}{3}\,\ell n\,\frac{V}{V_o}\ . \qquad \text{(A-7)}$$

APPENDIX B

Kuhlmann-Wilsdorf's Theory of Stage II Hardening[17]

It is well known that the rate of work hardening in single crystals is greatest in stage II, as illustrated in Figure B-1. The slope $\frac{\alpha\tau}{\alpha\gamma}$ in stage II is referred to as θ_{II} while $\frac{G}{\theta_{II}}$ is signified by K_{II}, where G is the rigidity modulus. Kuhlmann-Wilsdorf[17] points out that K_{II} is approximately equal to 300 in a great number of materials within a factor of two either way. She proposed that the most important contribution to work hardening is the reaction of dislocations against bowing out, due to their line stress. Her arguments are as follows.

When the dislocation density rises, the average free dislocation length $\bar{\ell}$ is decreased. This raises the flow stress since

$$\tau_{\bar{\ell}} = \frac{Gb}{h\bar{\ell}} \tag{B-1}$$

where b is the Burgers vector and h is an adjustable parameter. The average distance between dislocation can be considered as $c\bar{\ell}$ where c is a number between 1 and 2. A loop emitted from a dislocation segment will spread into a loop of radius $c\bar{\ell}$ before coming into contact with other dislocations. It will spread to an average radius, $r_{\bar{\ell}} = \alpha\, c\bar{\ell}$, before stopping if only the fraction $\frac{1}{\alpha}$ of all dislocations are positioned in such a manner that they can stop spreading loops. The number, dn, of newly-formed loops per unit volume will contribute to the increase in shear strain and

$$d\gamma = dnbhr_{\bar{\ell}}^{2} = dnbh\,(\alpha c\bar{\ell})^{2} \tag{B-2}$$

The dislocation density in a crystal can be assumed to be

$$\rho = \frac{m}{\bar{\ell}^{2}} \tag{B-3}$$

where m is a number depending on the actual dislocation distribution. The dn newly-formed loops add to the density

$$d\rho = dn\beta 2\pi r_{\bar{\ell}} \tag{B-4}$$

where β is a number between 0 and 1. The fraction β is necessary in order to account for the portion of dislocations which are mutually annihilated when dislocations of opposite Burgers vectors come into contact. By differentiating (B-3) and equating to (B-4) it is seen that

$$d\rho = -2m \frac{d\bar{\ell}}{\bar{\ell}^3} = 2h\beta r_{\bar{\ell}} dn = 2h\beta\alpha c\bar{\ell} dn \qquad \text{(B-5)}$$

and

$$dn = -\frac{m d\bar{\ell}}{h\beta\alpha c\bar{\ell}^4} \qquad \text{(B-6)}$$

By inserting equation (B-6) into (B-2) it is seen that

$$d\gamma = -\frac{mb\alpha c}{\beta} \frac{d\bar{\ell}}{\bar{\ell}^2} \qquad \text{(B-7)}$$

Differentiating equation (B-1) yields that

$$-\frac{d\bar{\ell}}{\bar{\ell}^2} = \frac{h}{Gb} d\tau_{\bar{\ell}} \qquad \text{(B-8)}$$

and $d\gamma$ is related to $d\tau_{\bar{\ell}}$ by the equation

$$d\gamma = \frac{hm\alpha c}{G\beta} d\tau_{\bar{\ell}} \qquad \text{(B-9)}$$

Since $\tau_{\bar{\ell}}$ is the important contribution to work hardening,

$$\theta_{II} \approx \frac{d\tau_{\bar{\ell}}}{d\gamma} = \frac{G\beta}{hm\alpha c} \qquad \text{(B-10)}$$

and

$$K = \frac{G}{\theta_{II}} \approx \frac{hm\alpha c}{\beta} \qquad \text{(B-11)}$$

Kuhlmann-Wilsdorf points out that this expression does not contain the Burgers vector. Therefore, the theory applies to crystals where dislocations are arranged in tangles (such as for Ni described here) as well as to crystals of low stacking fault energy where dislocations are arranged in pile-ups.

CONCLUSIONS

1. A dislocation cell structure is formed in nickel shock loaded up to 250 kilobars which is similar in character to that found in nickel statically loaded at temperatures 195°K and below.

2. Cell size decreases with the following changes in deformation conditions: increasing strain, increasing stress, decreasing temperature, and increasing shock loading pressure. The latter condition is the most effective.

3. A microtwinning structure has been observed for the first time in nickel shock loaded to 350 kilobars pressure or greater. Under these same conditions long thin distorted regions parallel to {111} planes, as well as a dislocation background, were observed.

4. For specimens deformed under initially ambient temperature conditions it is found that the energy input per unit volume is inversely proportional to the square of the average cell diameter. The energy required to obtain a given cell diameter decreases with decreasing temperature.

5. It has been shown that by the use of Kuhlmann-Wilsdorf's theory of work hardening[17] one can relate the energy per unit volume to the inverse square of the average width of active dislocation segments by means of a temperature dependent proportionality constant.

6. Using an analysis similar to Kuhlmann-Wilsdorf's theory[17] and Venables' proposal[21] for the stress level required to initiate twinning from a dislocation segment, another energy dislocation segment relation was proposed for twinning which includes the stacking fault energy.

7. By the use of these two energy relationships a calculation predicted that the average dislocation segment was approximately $\frac{1}{4}$ the size of the

average cell diameter. Also, the ratio between the rigidity modulus and the work hardening coefficient in stage II of work hardening was predicted. The value obtained corresponded extremely well with the experimental value obtained from Haasen's work[24] with nickel single crystals.

8. An attempt should be made to apply the analysis presented here to other metals. Perhaps if enough data were available it would be possible to make an estimate of the stacking fault energies of metals using this method.

Acknowledgments

The author wishes to extend his deep appreciation to Professor G. Thomas for his guidance throughout this entire research effort as well as his invaluable training in transmission electron microscopy techniques. The aid and cooperation of Arthur D. Little, Inc., especially Drs. R. S. Davis and B. A. Stein, through the donation of materials and shock loaded specimens as well as consulting services are also greatly appreciated. Others whom the author wishes to acknowledge and thank for their aid in various phases of the experimental work are Messrs. L. O. Seaborn, W. R. Goggin, A. E. Brown, O. Sommerville, Jr. and F. H. Brown. Thanks are extended to Miss S. Zuck for her special efforts in the typing of this thesis, and to the Inorganic Materials Research Division of the Lawrence Radiation Laboratory, under contract to the Atomic Energy Commission, who supported this project.

References

1. G. I. Taylor, "The Plastic Wave in a Wire Extended by an Impact Load," in The Scientific Papers of G. I. Taylor, Vol. I: The Mechanics of Solids, ed. by G. I. Batchelor, Cambridge University Press.

2. T. von Karman and P. Duwez, "The Propagation of Plastic Deformation in Solids," J. of Appl. Phys., 21, pp. 987-994 (1950).

3. K. A. Rakhmatulin, "Propagation of a Wave of Unloading," ONR Translation No. 2, Grad. Div. of Appl. Math., Brown University, Nov. 1948.

4. L. E. Malvern, "The Propagation of Longitudinal Waves of Plastic Deformation in a Bar of Material Exhibiting a Strain-rate Effect," J. of Appl. Mech., 18, pp. 203-208 (1951).

5. J. E. Dorn and F. E. Hauser, "Dislocation Concepts of Strain Rate Effects," Symposium of Structure Dynamics under High Impulsive Loading, Sponsored by NASA and WADD, September 17, 1962, Dayton, Ohio, to be published.

6. G. E. Dieter, "Metallurgical Effects of High-Intensity Shock Waves in Metals," Response of Metals to High-Velocity Deformation, ed. by P. G. Shewmon and V. F. Zackay, Interscience Publishers, New York, 1961, pp. 409-445.

7. W. C. Leslie, E. Hornbogen, and G. E. Dieter, "The Structure of Shock-Hardened Iron Before and After Annealing," J. Iron Steel Inst., 200, pp. 622-633 (1962).

8. G. Thomas, Transmission Electron Microscopy of Metals, John Wiley and Sons, New York, 1962, pp. 154-156.

9. Electron Microscopy and Strength of Crystals, ed. by G. Thomas and J. Washburn, Interscience Publishers, New York, 1963.

10. C. S. Smith, "Metallographic Studies of Metals After Explosive Shock," Trans. AIME, 212, pp. 574-589, (1958).

11. E. Hornbogen, "Shock-Induced Dislocations," Acta Met., 10, pp. 978-980 (1962).

12. J. E. Bailey, "Electron Microscope Observations on Recovery and Recrystallization Processes in Cold Worked Metals," Electron Microscopy and Strength of Crystals, ed. by G. Thomas and J. Washburn, Interscience Publishers, New York, 1963, pp. 535-574.

13. J. L. Walter and E. F. Koch, "Electron Microscope Study of Cold-Rolled and Annealed (100) [001] Crystals of High-Purity Silicon Iron," Acta Met., 10, pp. 1059-1075 (1962).

14. D. H. Warrington, "Dislocation Substructure in Polycrystalline Copper (As a Function of Temperature and Flow Stress)," Proceedings of the European Regional Conference of Electron Microscopy, Delft, 1960, pp. 354-357.

15. C. S. Barrett, Structure of Metals, McGraw-Hill, New York, 1952, p.494.

16. A. S. Keh and S. Weissmann, "Deformation Substructure in Body-Centered Cubic Metals," Electron Microscopy and Strength of Crystals, ed. by G. Thomas and J. Washburn, Interscience Publishers, New York, 1963 pp. 231-300.

17. D. Kuhlmann-Wilsdorf, "A New Theory of Work Hardening," Trans. of AIME, 224, pp. 1047-1061 (1962).

18. M. H. Rice, R. G. McQueen, and J. M. Walsh, "Compression of Solids by Strong Shock Waves," Solid State Physics, Vol. 6 Academic Press, New York, 1959, pp. 1-63

19. P. R. Thornton and T. E. Mitchell, "Deformation Twinning in Alloys at Low Temperatures," Phil. Mag., 7, pp. 361-375 (1962).

20. G. E. Dieter, "Hardening Effect Produced with Shock Waves," Strengthening Mechanisms in Solids, A. S. M. Seminar, American Society for Metals, Metals Park, Ohio, 1962, pp. 279-340.

21. J. A. Venables, "Deformation Twinning in Face-Centered Cubic Metals," Phil. Mag., 6, pp. 379-396 (1961).

22. H. Suzuki and C. S. Barrett, "Deformation Twinning in Silver-Gold Alloys," Acta Met., 6, pp. 156-165 (1958).

23. J. B. Cohen and J. Weertman, "A Dislocation Model for Twinning in F.C.C. Metals," Acta Met., to be published.

24. P. Haasen, "Plastic Deformation of Nickel Single Crystals at Low Temperatures," Phil. Mag., 3, pp. 384-418 (1958).

25. D. S. Wood, "On Longitudinal Plane Waves of Elastic-Plastic Strain in Solids," J. Appl. Mechanics, 19, pp. 521-525 (1952).

26. A. H. Holtzman and G. R. Cowman, "The Strengthening of Austenitic Manganese Steel by Plane Shock Waves," Response of Metals to High Velocity Deformation, ed. by P. G. Skewmon and V. F. Zackay, Interscience Publishers, New York, 1961, pp. 447-482.

List of Illustrations

Figure 1. Specimen Assembly for Shock Loading.

Figure 2. Wire Tool for Spark Erosion Cutting Technique.

Figure 3. Vickers Hardness vs. Loading Pressure for Shock Loaded and Compressive Specimens.

Figure 4. Plot of Vickers Hardness vs. Shock Pressure for Nickel Obtained from Data of Dieter.[5]

Figure 5. Electron Micrograph of Annealed Specimen (Spark erosion cutting used in preparation).

Figure 6a-c. Electron Micrographs of Shock Loaded Specimens Showing Cell Structure: (Shock direction lies in plane of foil).

a. 70 Kilobar Specimen (Shock direction indicated by arrow marked C)

b. 130 Kilobar Specimen (Shock direction indicated by arrow marked C)

c. 250 Kilobar Specimen

Figure 7. High Magnification Electron Micrograph of 250 Kilobar Specimen Showing Cell Structure (Shock direction lies in plane of foil).

Figure 8. Electron Micrograph of 350 Kilobar Specimen on (110) Plane Showing Twinning Structure and Dislocation Background (Shock direction lies in plane of foil).

Figure 9a. Selected Area Diffraction Pattern of Region Shown in Figure 9b.

9b. Electron Micrograph of 350 Kilobar Specimen on $(5\bar{1}0)$ Plane Showing Twinning Structure (Shock direction lies in plane of foil as indicated by arrow marked C).

Figure 10. Electron Micrograph of 350 Kilobar Specimen on (112) Plane Showing Long Thin Distorted Region and Dislocation Background (Shock direction lies in plane of foil as indicated by arrow C).

Figure 11a. Electron Micrograph of 350 Kilobar Specimen on (112) Plane Showing Long Thin Distorted Region (Shock direction lies in the plane of foil).

11b. Selected Area Diffraction of Region Shown in Figure 11a.

Figure 12. Electron Micrograph of Specimen Compressively Strained 10% (Compressive direction lies in the plane of the foil).

Figure 13. Electron Micrograph of Specimen Compressively Strained 60% (Compressive direction lies in plane of foil as indicated by arrow marked C).

Figure 14. Electron Micrograph on (001) Plane of Tensile Specimen Strained 20% at 295°K (Tensile direction in plane of foil).

Figure 15. Electron Micrograph on (001) Plane of Tensile Specimen Strained 20% at 78°K (Tensile direction in plane of foil).

Figure 16. Plot of Inverse Square of Cell Diameter vs. Work per Unit Volume.

Figure 17. Plot of Cell Diameter vs. Temperature.

Figure 18. Electron Micrograph of Compressive Specimen Strained 10% Indicating Dislocations Bowing Out from Cell Wall (Compressive direction in plane of foil).

Figure A-1. Hugoniot Curve for Nickel.[17]

Figure A-2. General Approximation of Pressure-Strain Curve for Shock Loaded Metal.

Figure B-1. Typical Single Crystal Stress-Strain Curve.

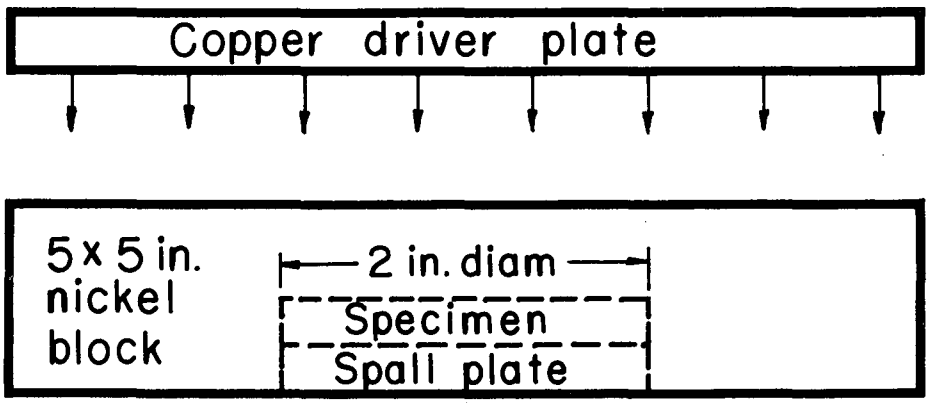

MU-30485

Fig. 1

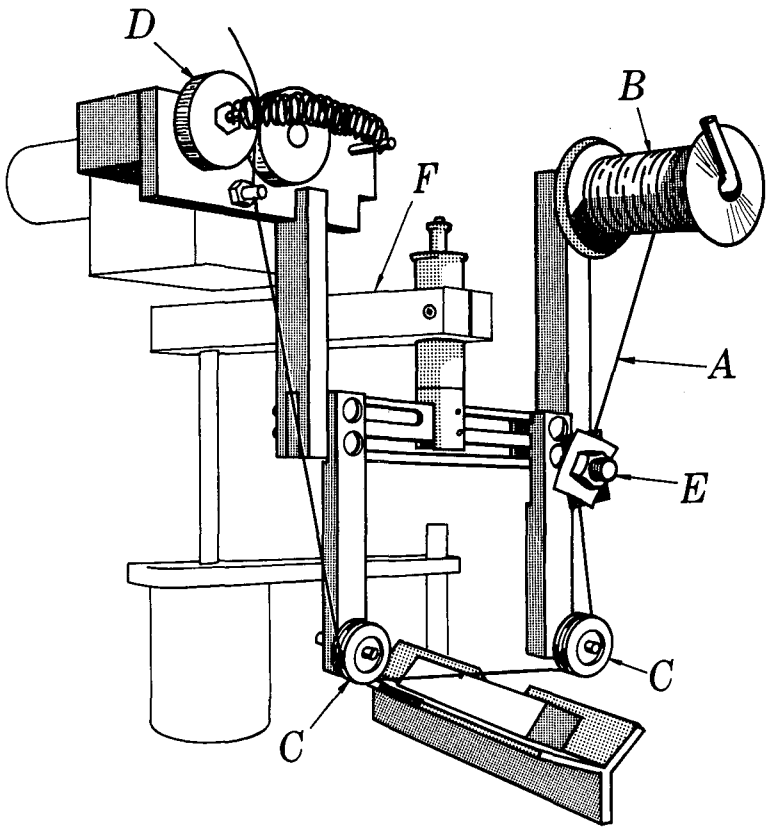

MU-27002

Fig. 2

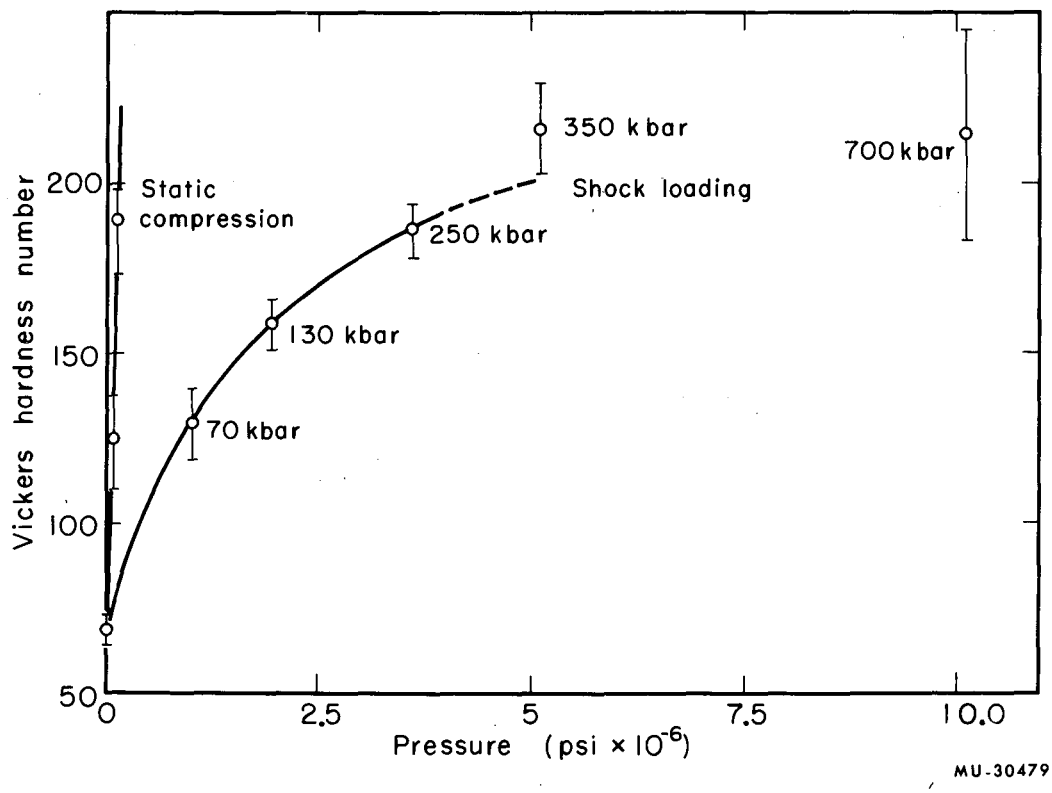
Vickers hardness number
200
150
100
50
0
2.5
5
7.5
10.0
Pressure (psi × 10^-6)
Static compression
70 kbar
130 kbar
250 kbar
350 k bar
Shock loading
700 k bar
MU-30479

Fig. 3

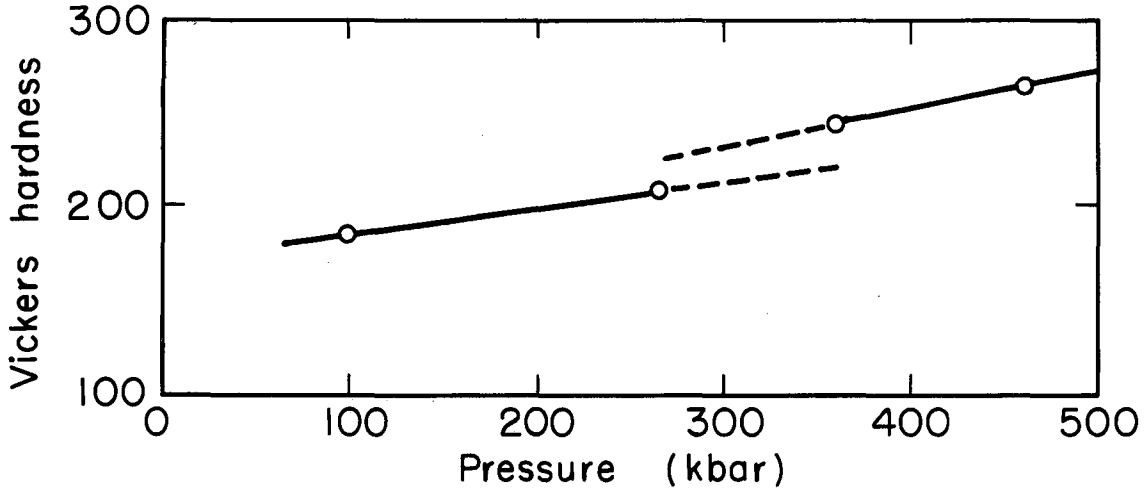

MU-30480

Fig. 4

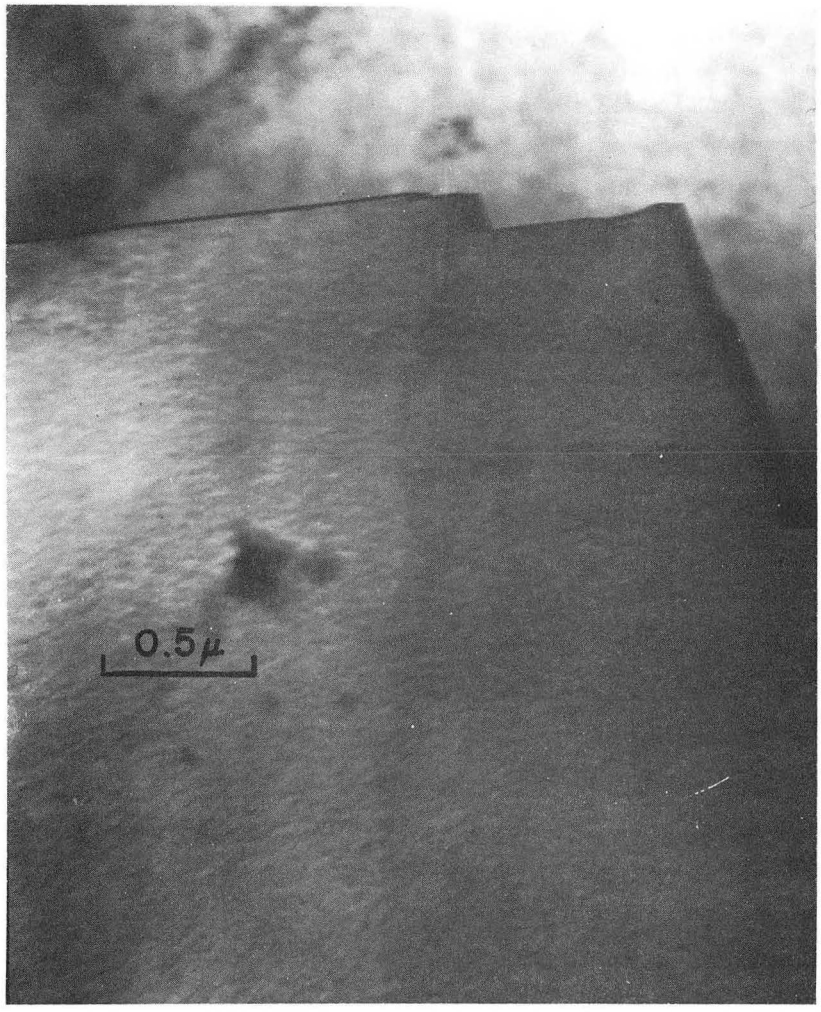

ZN-3762

Fig. 5

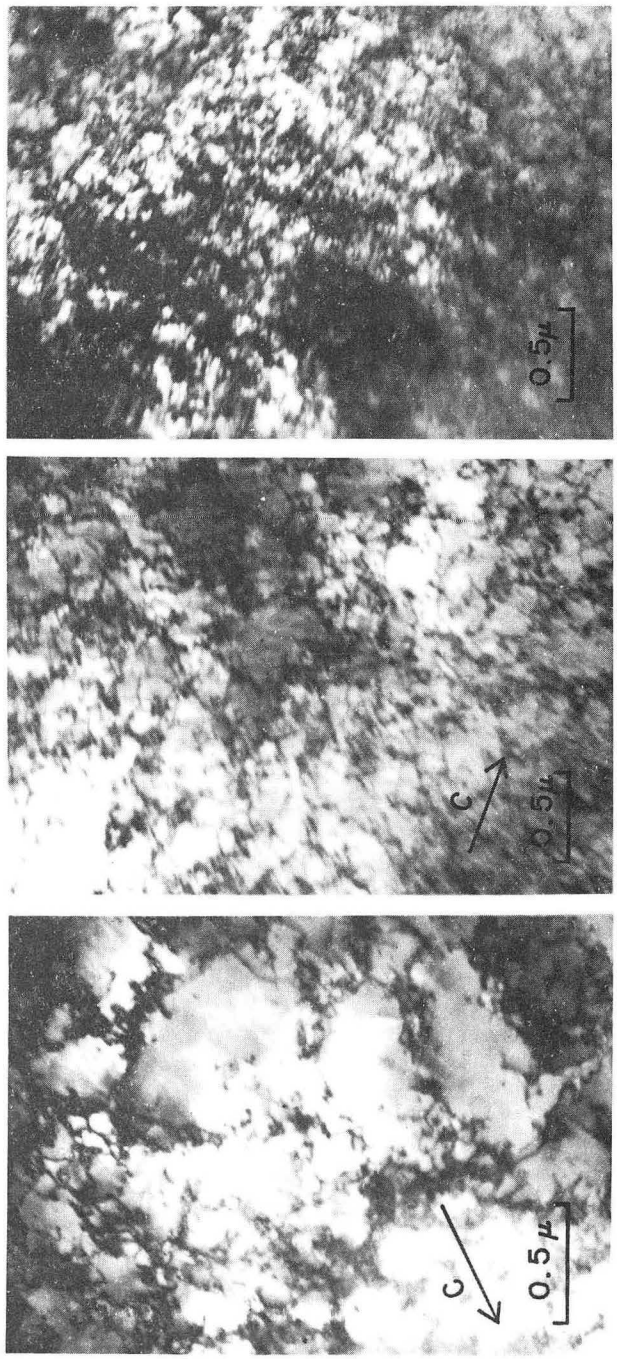

(a) (b) (c)

ZN-3785

Fig. 6

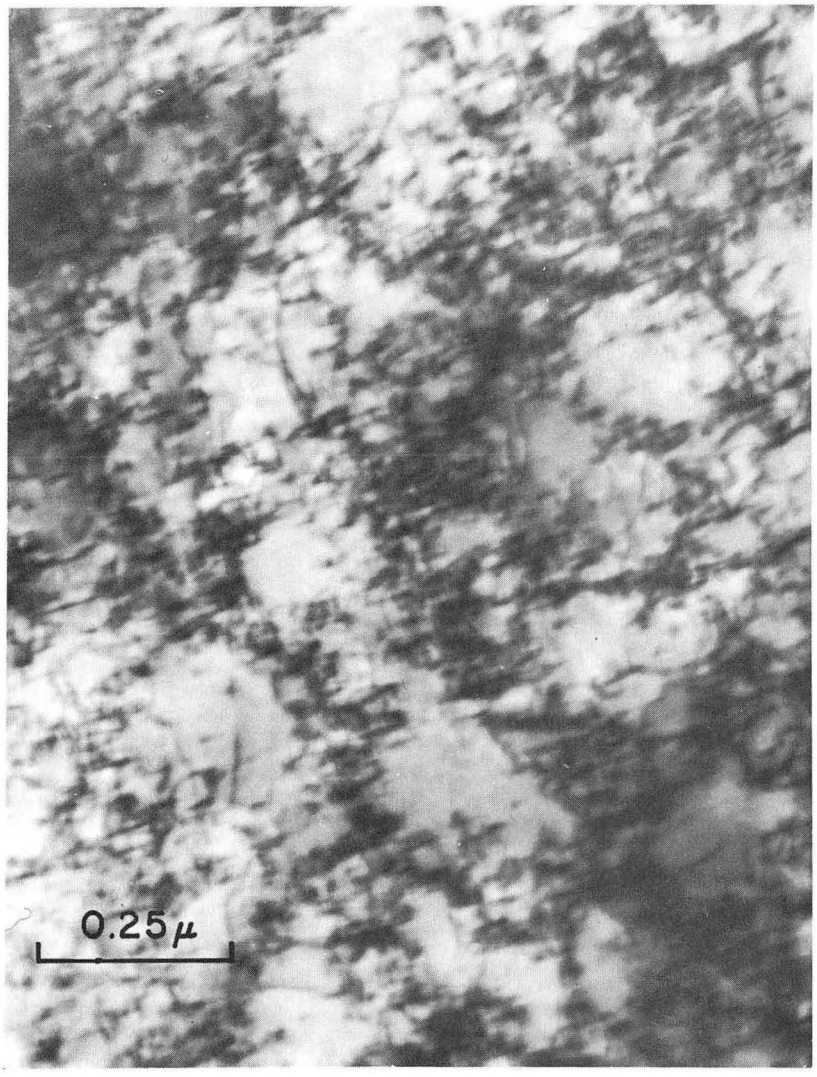

ZN-3761

Fig. 7

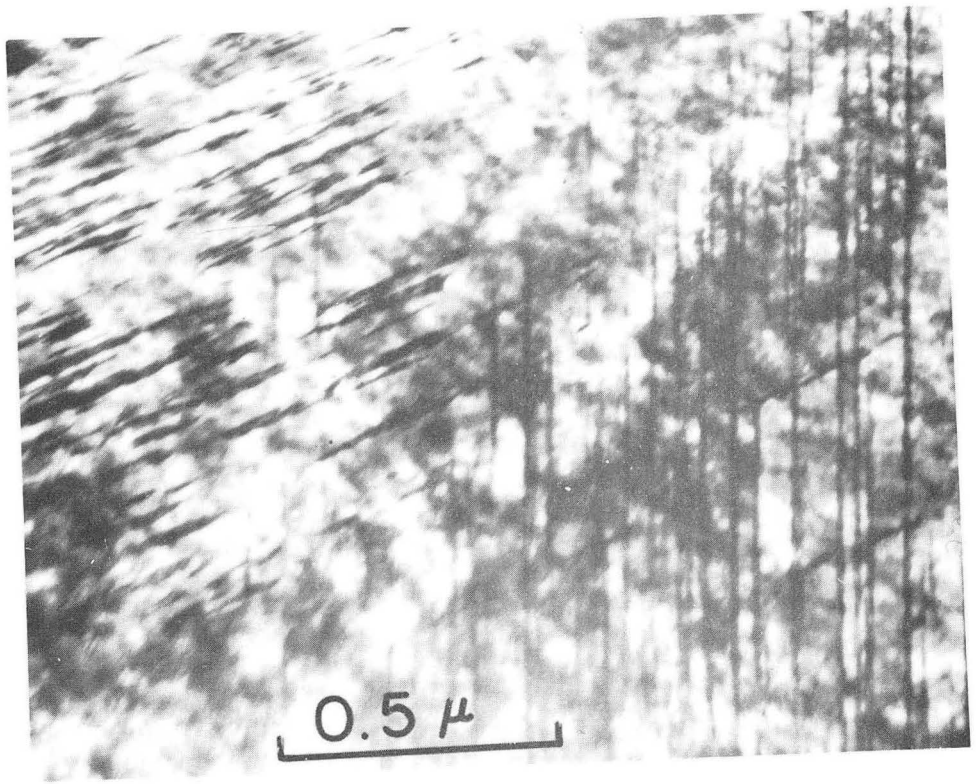

ZN-3566

Fig. 8

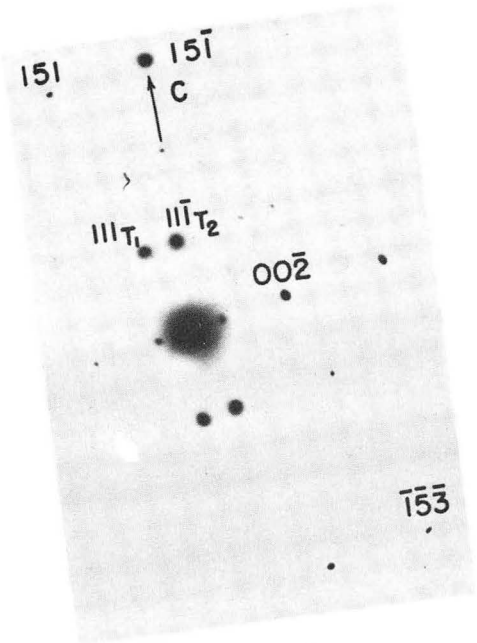

(a)

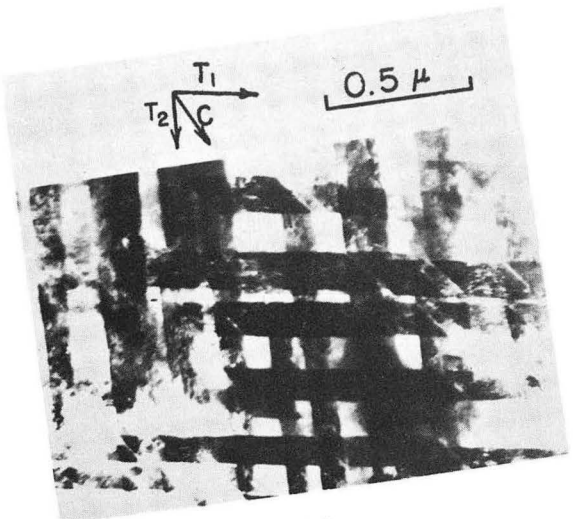

(b)

ZN-3786

Fig. 9

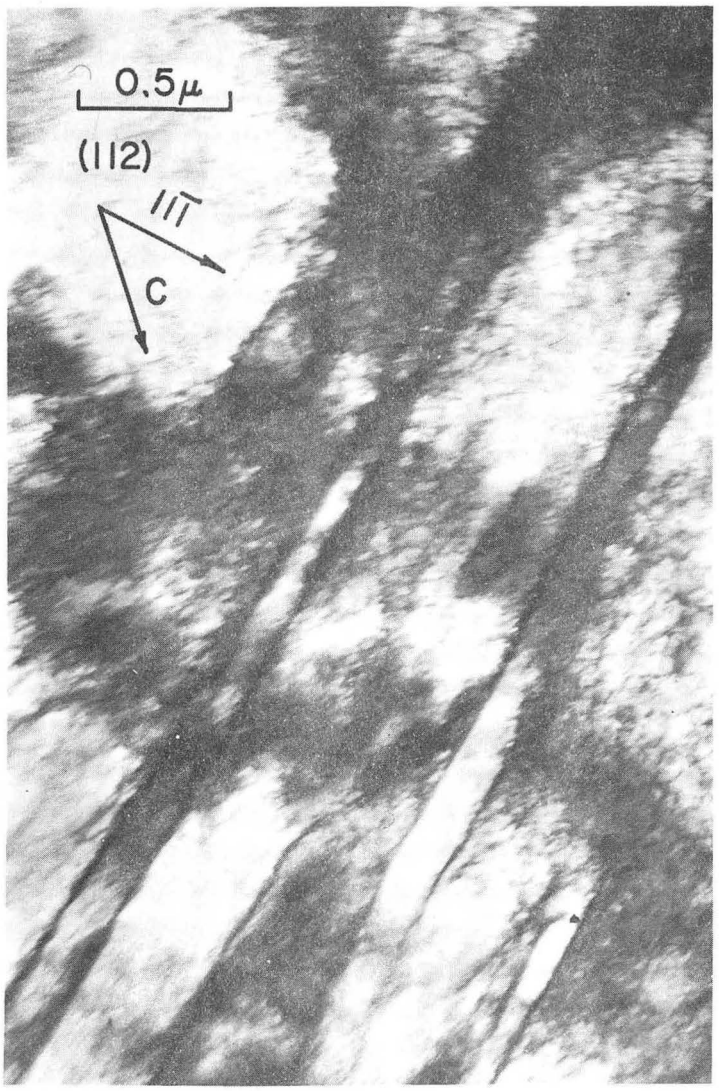

ZN-3760

Fig. 10

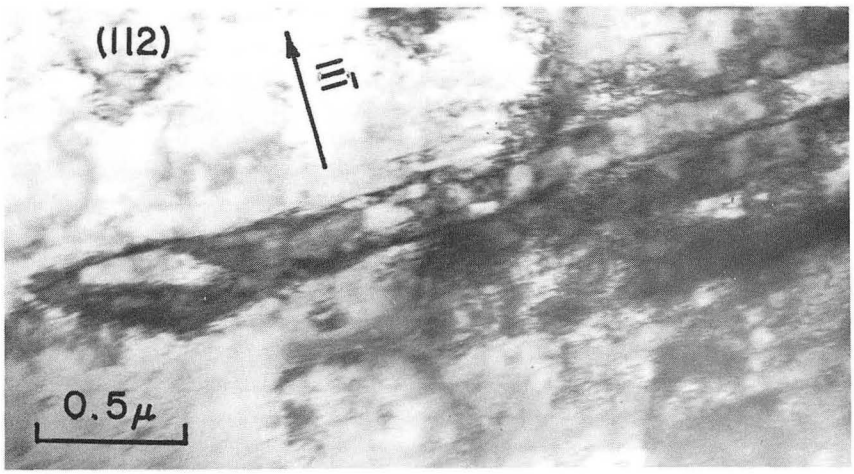

(a)

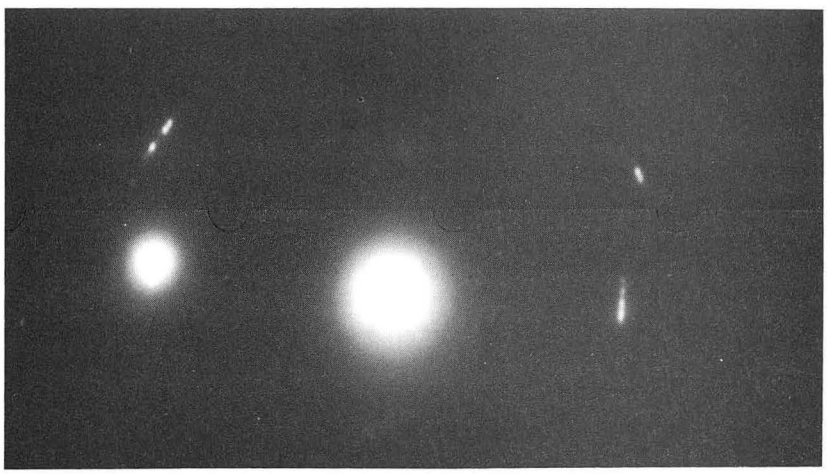

(b)

ZN-3787

Fig. 11

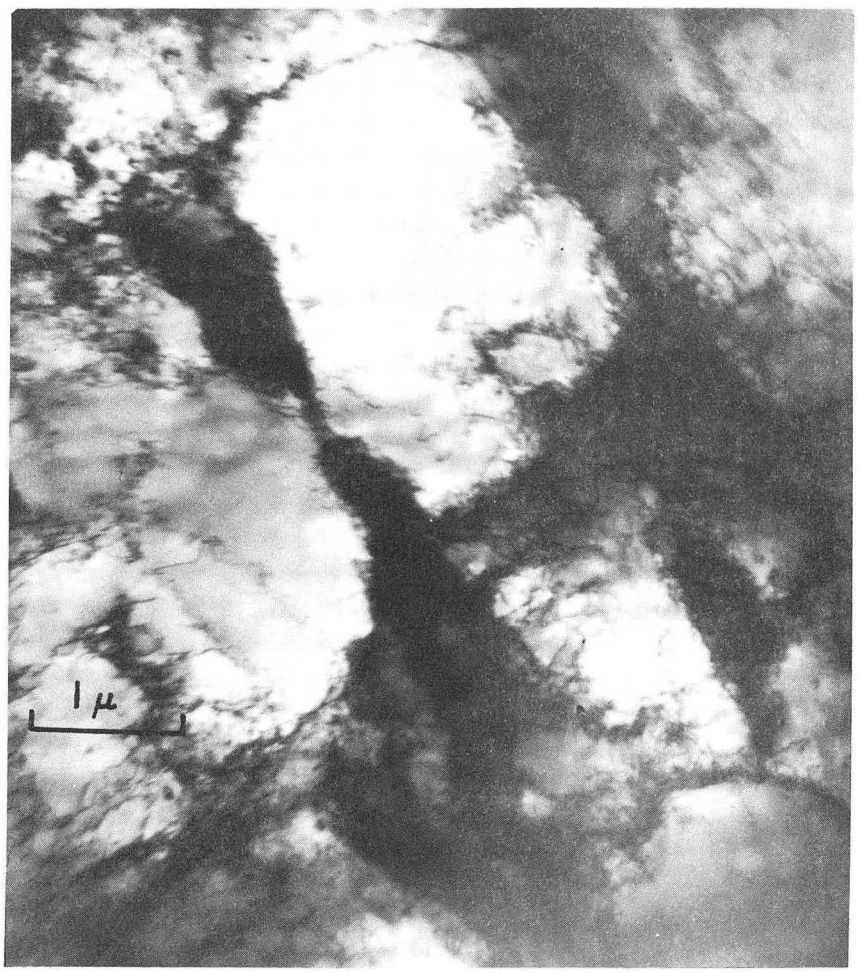

ZN-3765

Fig. 12

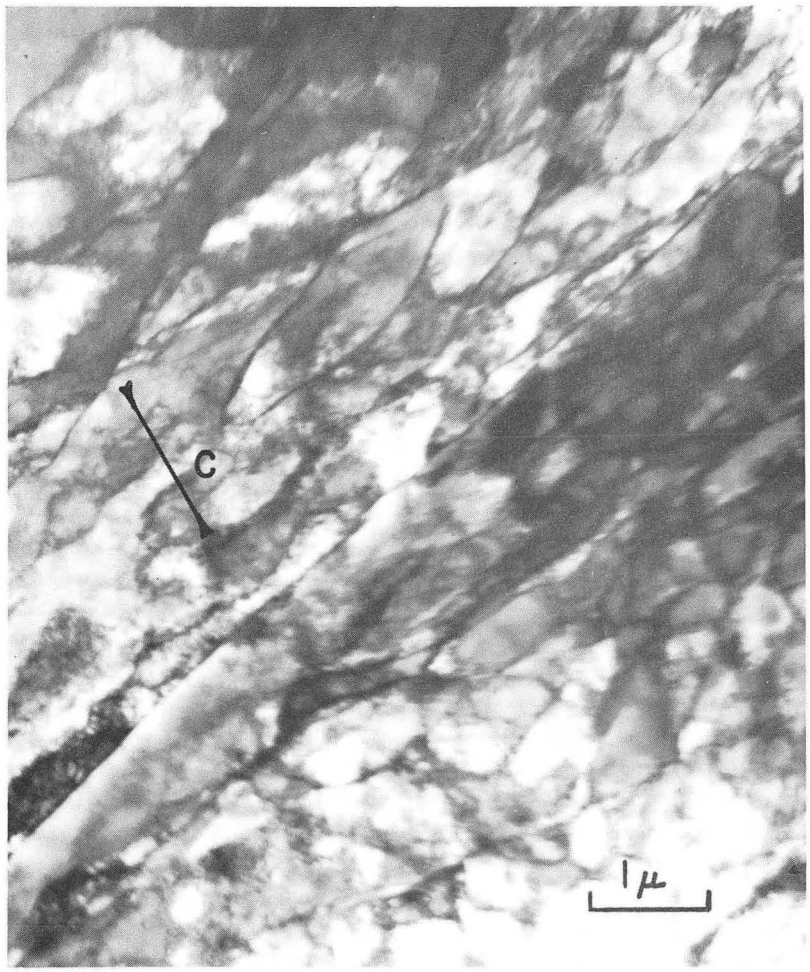

ZN-3759

Fig. 13

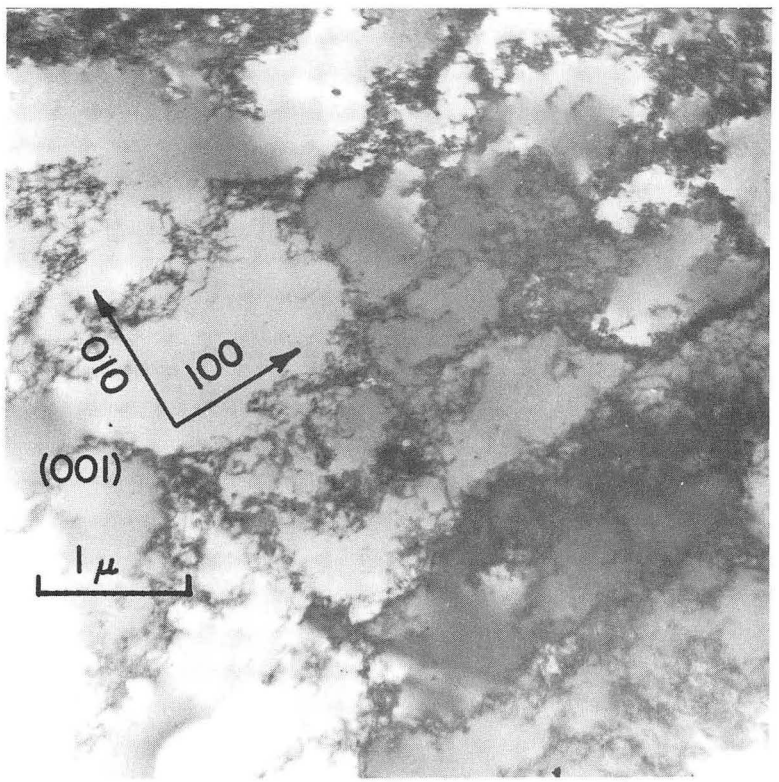

ZN-3764

Fig. 14

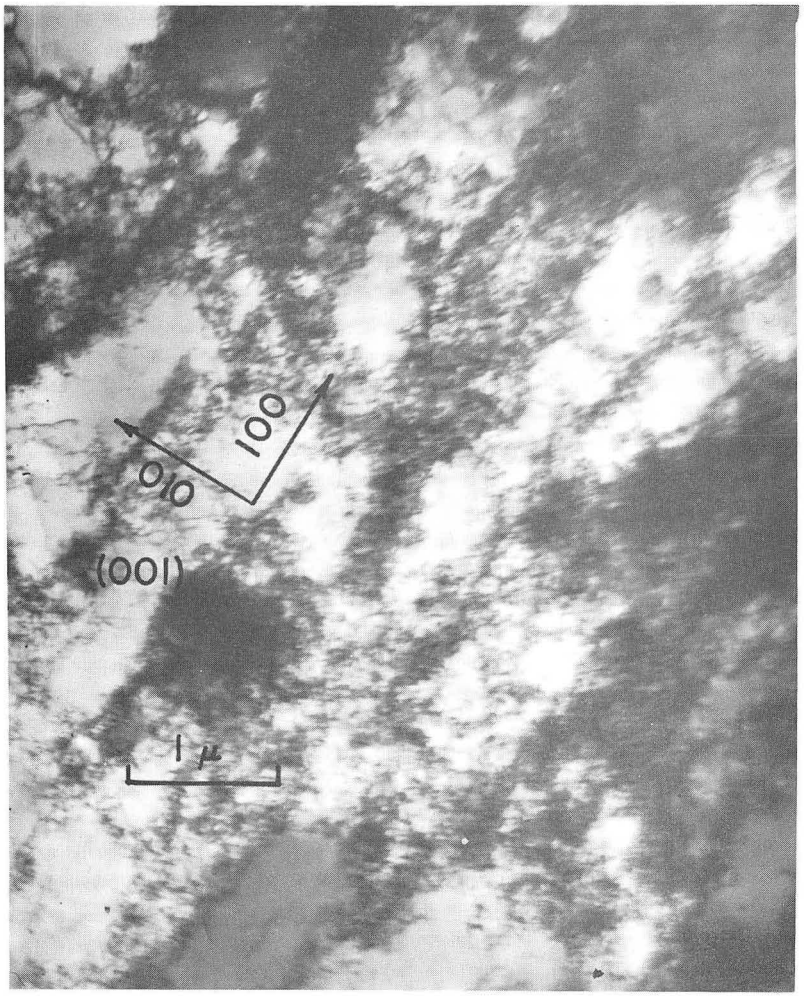

ZN-3766

Fig. 15

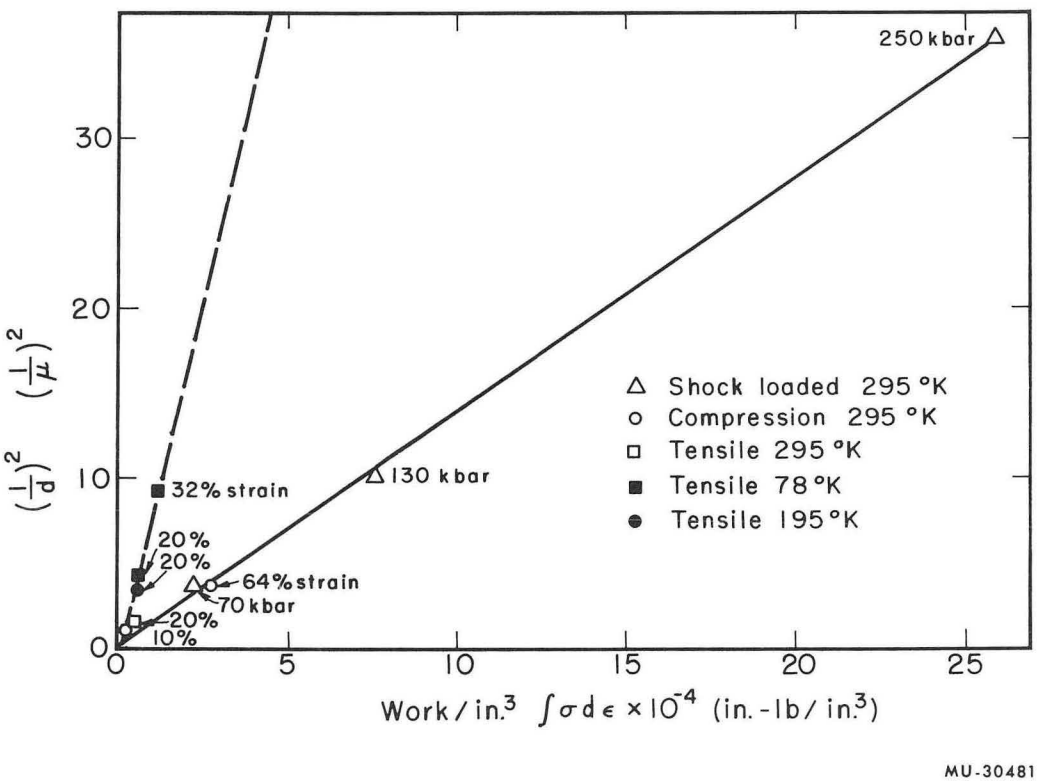
250 kbar
130 kbar
32% strain
20%
20%
64% strain
70 kbar
20%
10%
Shock loaded 295 °K
Compression 295 °K
Tensile 295 °K
Tensile 78 °K
Tensile 195 °K
$\left(\frac{1}{d}\right)^2$ $\left(\frac{1}{\mu}\right)^2$
Work / in.^{3} $\int \sigma d\epsilon \times 10^{-4}$ (in.-lb/ in.^{3})
0
10
20
30
0
5
10
15
20
25
MU-30481

Fig. 16

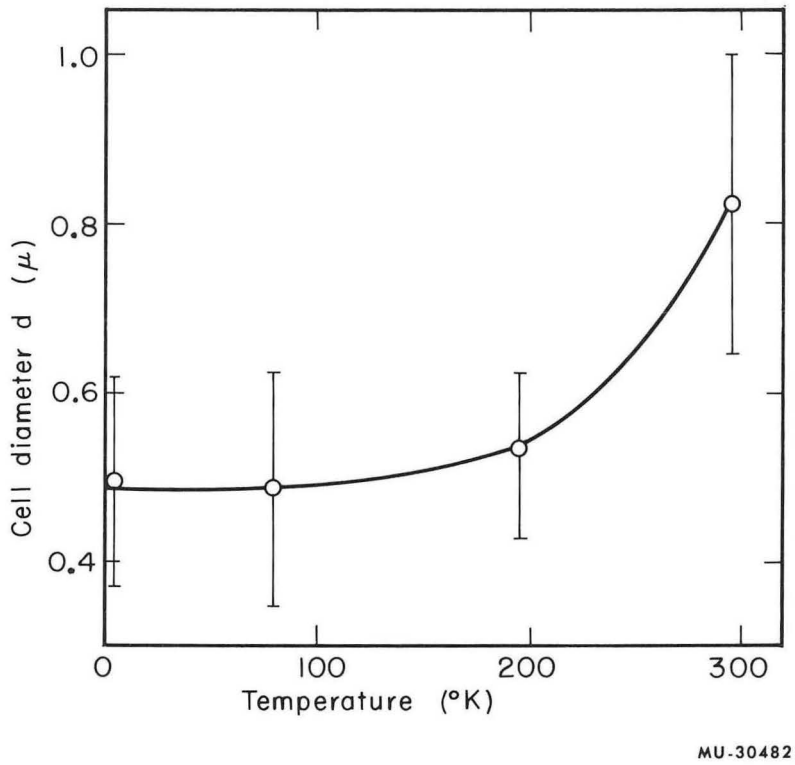
1.0
0.8
0.6
0.4
Cell diameter d (μ)
0
100
200
300
Temperature (°K)
MU-30482

Fig. 17

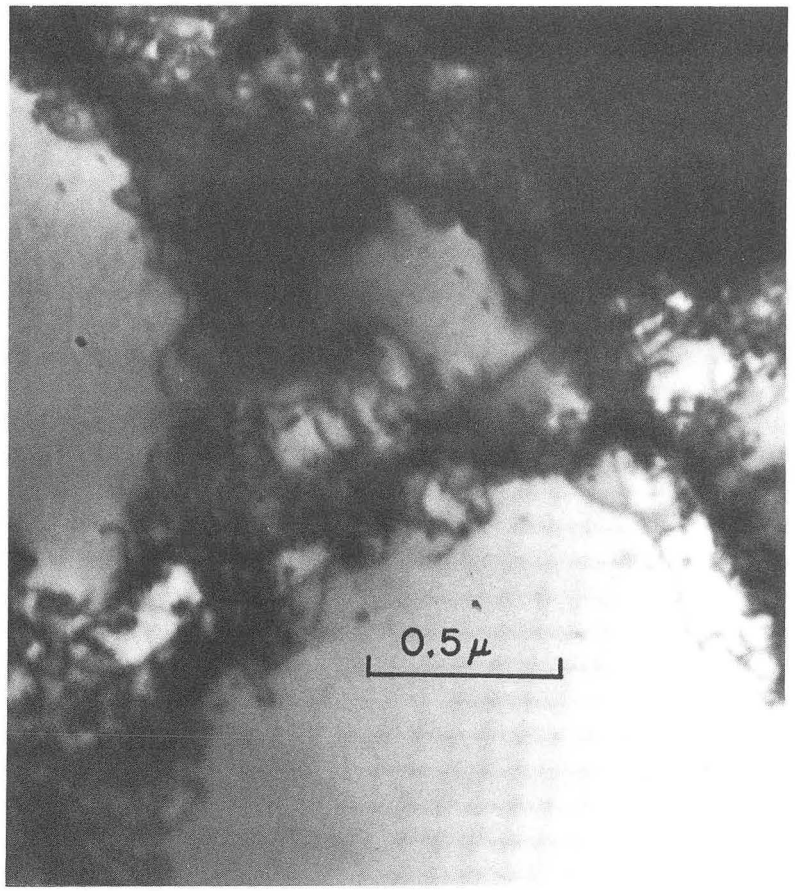

ZN-3763

Fig. 18

Hugoniot curve
for nickel (Ref. 17)

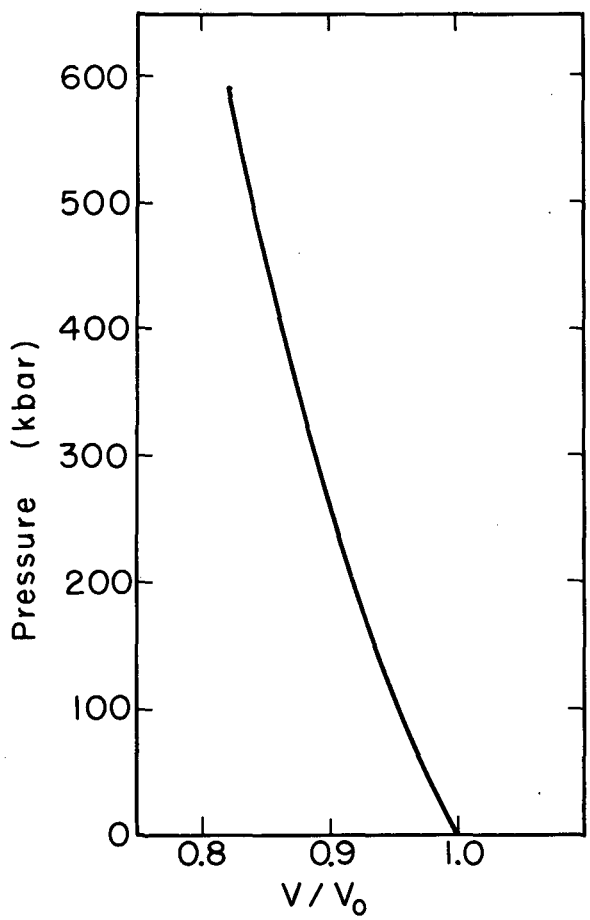

MU-30483

Fig. A-1

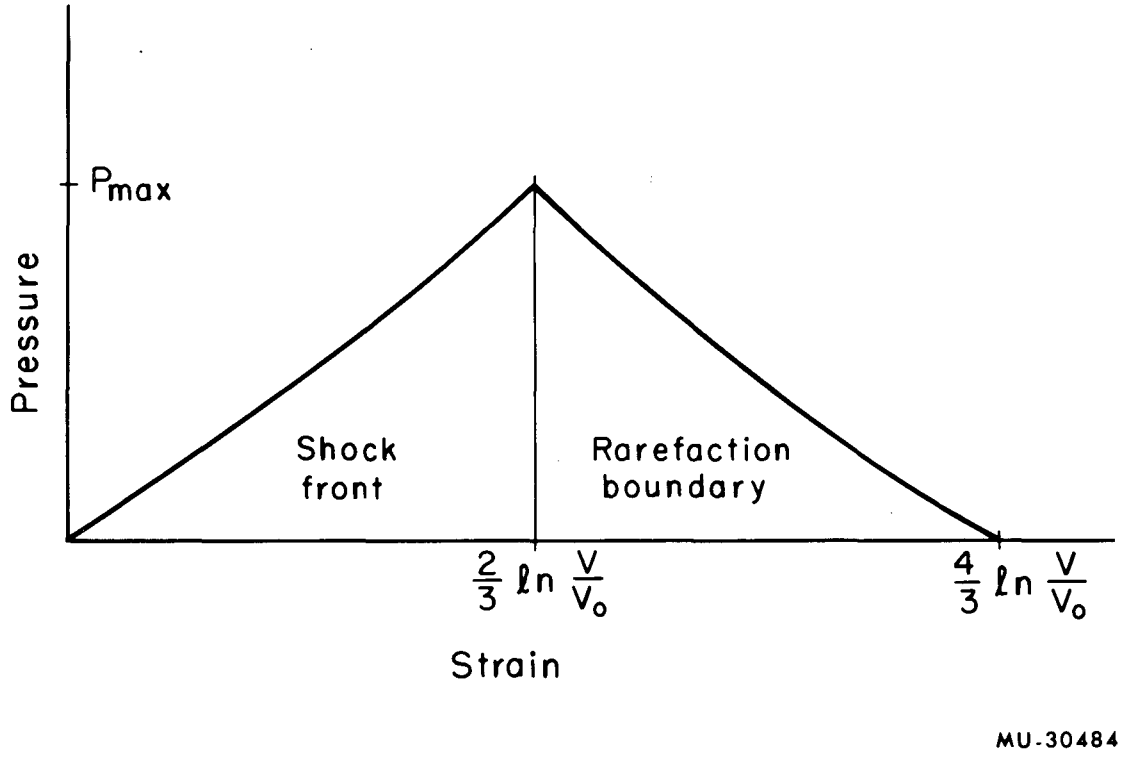
Pmax
Pressure
Shock front
Rarefaction boundary
2/3 ln V/Vo
4/3 ln V/Vo
Strain
MU-30484

Fig. A-2

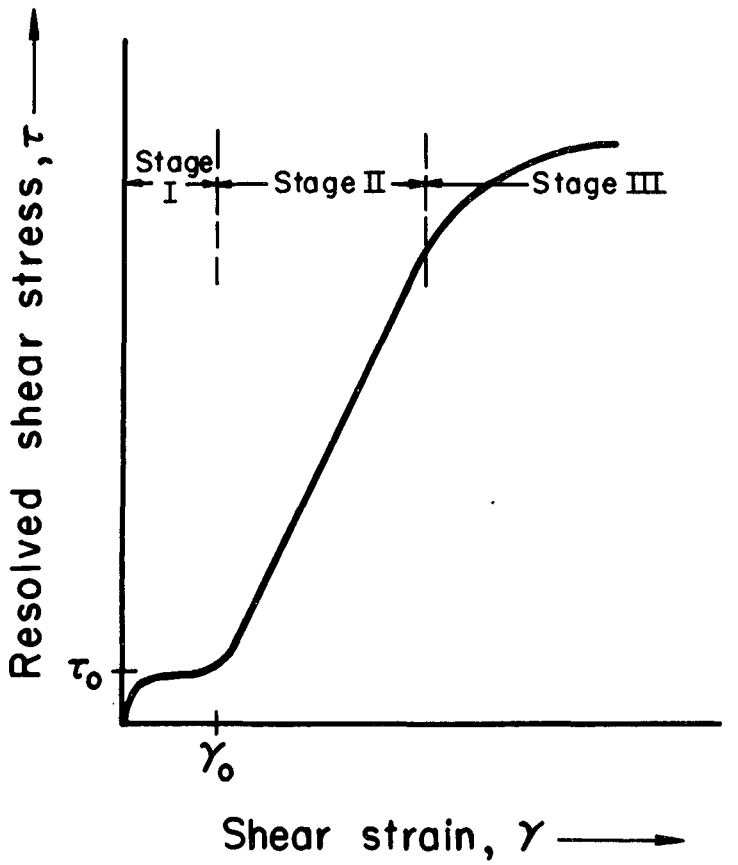

MU-30486

Fig. B-1

LEGAL NOTICE

This report was prepared as an account of Government sponsored work. Neither the United States, nor the Commission, nor any person acting on behalf of the Commission:

A. Makes any warranty or representation, expressed or implied, with respect to the accuracy, completeness, or usefulness of the information contained in this report, or that the use of any information, apparatus, method, or process disclosed in this report may not infringe privately owned rights; or

B. Assumes any liabilities with respect to the use of, or for damages resulting from the use of any information, apparatus, method or process disclosed in this report.

As used in the above, "person acting on behalf of the Commission" includes any employee or contractor of the commission, or employee of such contractor, to the extent that such employee or contractor of the Commission, or employee of such contractor prepares, disseminates, or provides access to, any information pursuant to his employment or contract with the Commission, or his employment with such contractor.